

VCST Internal Memo

Title: Improvement in the Characterization of the SDSM Solar Screen Vignetting Function

Memo Number: 2013_001

Revision: 01

Date: February 15, 2013

Author: Jeff McIntire and Boryana Efremova

To: Xiaoxiong Xiong and James Butler

Cc: Hassan Oudrari, Kwo-Fu (Vincent) Chiang, Jon Fulbright and Aisheng Wu

References

- [1] Jeff McIntire, Boryana Efremova, and Junqiang Sun, "Preliminary Analysis of VIIRS F1 Yaw Maneuver Data", VCST_TECH_REPORT_12_008, February 23, 2012.
- [2] Jeff McIntire, Boryana Efremova, Jon Fulbright, and Jack Xiong, "VIIR F1 SDSM Screen Transmission as Determined from Yaw Maneuver Data", VCST_TECH_REPORT_12_012, March 15, 2012.
- [3] Jeff McIntire and Boryana Efremova, "Determination of NPP VIIRS Vignetting Functions for the SDSM Based on Yaw Maneuver Data", VCST_TECH_MEMO_12_023, September 17, 2012.
- [4] Jeff McIntire, Boryana Efremova, Jon Fulbright, and Jack Xiong, "VIIRS F1 SDSM Screen Transmission Investigation", VCST_TECH_REPORT_12_010, May 8, 2012.

1. Introduction

An updated SDSM solar screen vignetting function was derived based on yaw maneuver analysis [1-3]. This screen update was delivered for implementation in the operational SDR processing on March 15, 2012. While the H factor was significantly improved both in terms of magnitude and variability, some short timescale variation remained. These remaining variations are the result of unresolved features in the SDSM solar screen vignetting function that were not captured by the coarse sampling in the horizontal angle provided by the yaw maneuver data.

The focus of this memo is to produce a vignetting function for the SDSM solar screen with sufficient resolution to remove the short term variability remaining in the H factor. Non-yaw data is incorporated into the analysis to fill the gaps in the sampling of the horizontal angle (SDSM azimuth). A preliminary investigation into this method was presented in [4]. Section 2 will establish the analysis methodology and Section 3 will discuss the results of this analysis.

2. Methodology

The SDSM screen transmission derived on-orbit using yaw maneuver data was described in [3]; the same basic process is repeated here. The irradiance incident on the SDSM detector is related to the detector voltage by

$$E = g_{SDSM} dc, \quad (1)$$

where g_{SDSM} is the SDSM detector gain, which can be determined from either SDSM view. In this work, we determine the gain from the SD view, or

$$g_{SDSM} - SD = \frac{\tau_{SAS} (H / H_0) BRF_{SDSM} \cos \theta_{SD} \sin^2 \psi E_{sun}}{dc_{SD}} . \quad (2)$$

Here BRF_{SDSM}/π is the initial SD BRDF at the SDSM reflectance angle (backscatter), $\pi \sin^2 \psi$ is the approximate solid angle of the entrance cone into the SDSM for the SD view, dc_{SD} is the voltage of the SDSM detectors for the SD view with the dark offset voltage subtracted, τ_{SAS} is the vignetting function of the SD screen, E_{sun} is the solar irradiance, and $\cos \theta_{SD}$ accounts for the projection of the solar footprint onto the SD. H is a measure of the relative degradation of the SD BRDF, and is normalized to the first measurement (H_0).

The SDSM is designed to ratio near-simultaneous measurements of solar illumination incident on its detectors from two separate views. This ratio is referred to as the H factor and is defined as

$$H = \frac{dc_{SD}}{dc_{sun}} \frac{\tau_{SDSM}}{\tau_{SAS} BRF_{SDSM} \cos \theta_{SD} \sin^2 \psi} , \quad (3)$$

where τ_{SDSM} is the SDSM solar screen vignetting function and dc_{sun} is the voltage of the SDSM detectors for the sun view with the dark offset voltage subtracted.

To determine the SDSM screen vignetting function, Eq. (4) is solved for τ_{SDSM} , or

$$\tau_{SDSM} = \frac{dc_{sun}}{dc_{SD}} \tau_{SAS} (H / H_0) BRF_{SDSM} \cos \theta_{SD} \sin^2 \psi . \quad (4)$$

Here the $\tau_{SAS} BRF_{SDSM}$ used in this calculation was determined in [3]. Note that the H factor is now normalized to H_0 .

The SAS and SDSM screens were misaligned when the instrument was assembled; as such the range of angles available for use in the calibration becomes more restricted as the SDSM screen azimuth becomes larger. This causes boundary effects during the calculation of the SDSM screen transmission using Eq. (4). The SDSM screen transmission as determined by Eq. (4) uses an instantaneous detector gain. For regions of the screen transmission where data is lacking, an average orbital gain is used (which is defined in Eq. (2) averaged over all valid scans in an orbit). The SDSM screen transmission as defined using the average orbital gain is

$$\tau_{SDSM} = g_{SDSM} - SD \frac{dc_{sun}}{E_{sun}} . \quad (5)$$

This approach is applied to both yaw and non-yaw data. The yaw data was described in [3]. The non-yaw data selected is a set of orbits covering the yearly variation in SDSM azimuth angle. Then the τ_{SDSM} is derived from both yaw and non-yaw data sets.

The H factors are fit over the entire mission to a function of the form

$$\left(\frac{H}{H_0} \right) = A_0 e^{-A_1 X} + 1 - A_0 \quad (6)$$

where A_0 and A_1 are free parameters and X is the orbit number. The H factors used here were determined using the screen updates defined in [3]. This functional form is then used to remove the SD degradation from the data used to determine τ_{SDSM} .

3. Analysis Results

3.1 Data Quality and Reduction

The data selection and reduction performed in the calculation of τ_{SDSM} is described in this section. The angle ranges of -14.5 to +2.0 degrees in SDSM azimuth and -4 to +2.0 degrees in SDSM elevation were used to select the data from each orbit. The justification for these angle limits and the angle definitions are contained in [3].

NPP VIIRS has gone through its yearly cycle of SDSM azimuth, as shown in Figure 1 where the SDSM azimuth at 0 degrees SDSM elevation is graphed versus orbit (the yaw orbits are highlighted in red). In this work we investigate the use of two data sets covering the full yearly range of SDSM azimuth. The specific orbits used in both cases are listed in Table 1; note that some orbits were not included in the first set due to either repeated data or quality issues such as eclipses or star tracker problems. The yaw maneuver data is also listed in Table 1. Figure 2 shows the SDSM azimuth at 0 degrees SDSM elevation graphed versus orbit with the selected data highlighted in green, upper plot for data set 1 and lower plot for data set 2. In the next section, the results from data set 1 are presented along with a comparison to data set 2 results. Note that a small section of data early in the mission was not included in data set 1 at higher azimuth angles; this is due to errors in the solar vector resulting from problems with the star tracker.

As in [3], quality checks were performed on the individual SDSM samples to ensure no spurious data was included. The remaining SDSM data was averaged over samples for each scan, and then the dark offset was subtracted.

τ_{SDSM} was then computed and placed on a regular grid of 80 x 60 (SDSM azimuth x SDSM elevation) with step sizes of approximately 0.12 degrees SDSM azimuth and 0.10 degrees SDSM elevation. The angle limits used were SDSM azimuth of -14.5 to +2.0 degrees and SDSM elevation of -4 to +2 degrees. As in [3], some minor extrapolation was conducted, both to produce a rectangular map of the transmission factors and to provide a small buffer in case the solar azimuth angle exceeded expectations.

3.2 Results

The results of the τ_{SDSM} calculation are discussed in this section. The computed SDSM screen transmissions for SDSM detectors 1 – 8 are shown in Figures 3 – 10 (upper plots); here the screen transmissions were normalized to the highest point. Distinct ridges roughly constant in SDSM elevation are visible and τ_{SDSM} generally decreases with SDSM azimuthal angle. These ridges are more sharply defined in the current calculation as compared to previous results. The ratios of the delivered τ_{SDSM} [3] to the current derived τ_{SDSM} are shown in the lower plots of Figures 3 – 10. The delivered screen transmission did not characterize the distinct ridges in SDSM elevation as well, with differences of up

to $\pm 0.5\%$ for an individual point.

The (H/H_0) trends for all eight SDSM detectors from the beginning of the mission are shown in Figure 11. The upper plot shows the trend using the delivered transmission factors [3] and the lower plot shows the same trend using the τ_{SDSM} derived here. The variability, particularly in the higher number detectors is diminished through the use of the current transmission factors. There is still a slight bump in the lower plot around orbit 4500, which may result from a deficiency in the H factor model. Figure 12 plots the ratio (delivered / derived) of the H factors over the entire mission. Differences of up to 1 % for a given orbit are observed.

Figures 13 – 16 graph the scan-to-scan variation in the (H/H_0) trend versus orbit for SDSM detectors 1 – 8. The at-launch (black), delivered (red), and derived (blue) τ_{SDSM} are all plotted. Note that the scan-to-scan variation is improved for most orbits using the derived τ_{SDSM} in comparison to both the at-launch and delivered τ_{SDSM} . This indicates that the derived screen transmission is better characterized in both the vertical and horizontal angles. Note that the area of the derived screen transmission for which non-yaw data was lacking was equivalent to the delivered τ_{SDSM} .

As the SNPP mission has passed through its yearly orbit cycle in terms of SDSM azimuth, there are two data sets from which a screen transmission of this type can be derived (see Table 1). The results from the first data set have been discussed above; now those results are compared to the results using the second data set. Figure 17 shows the (H/H_0) trends using screen transmissions derived from both the first and second data sets (upper and lower plots, respectively). Figure 18 plots the ratio of the H factors from both calculations for all detectors. Here the differences are less than 0.5% for any given orbit. Also, it is important to note that the slight bump in the H factors changes position, indicating that that feature is not real but an artifact of the analysis. A direct comparison of the (H/H_0) trends for each SDSM detector is shown in Figures 19 – 22 where the delivered τ_{SDSM} , derived τ_{SDSM} using data set 1, and derived τ_{SDSM} using data set 2 are graphed in black, red, and blue respectively. There is more variation in the blue curves than the red, which may result from deviations from the model used to remove the SD degradation from the data incorporated into the screen transmission derivation. In addition, the scan-to-scan variation is greater when using the screen transmission derived from the second data set (not shown).

Note that in this work the derived τ_{SDSM} is SDSM detector dependent. The transmission of the screen itself should be achromatic; however, small geometric differences in the optical paths between the SDSM detectors inside the integrating sphere are captured in the detector dependent τ_{SDSM} and are non-negligible.

Note that this method relies on the H factor model in Eq. (6). As seen in Figures 19 – 22, model dependent features are still present and as such model uncertainty could be a significant contributor to the overall uncertainty.

4. Conclusions

Updates to the τ_{SDSM} using non-yaw data in addition to the yaw maneuver data were derived in this work. Orbital variations in the (H/H_0) have been reduced and scan-to-scan variations have also decreased. The results indicate that the screen transmission derived here improves the characterization of the on-orbit SD degradation, by better characterizing the fine structure of screen.

Table 1: Non-yaw data used in this work.

Data Set	Orbits
Set 1	289 – 394, 396 – 1434, 1497 – 1559, 1581 – 1750, 2500 – 3650
Set 2	3651 – 5250
Yaw	1560 – 1579

Figure 1: SDSM azimuth angle at 0 degrees SDSM elevation versus orbit. Yaw maneuver orbits are highlighted in red.

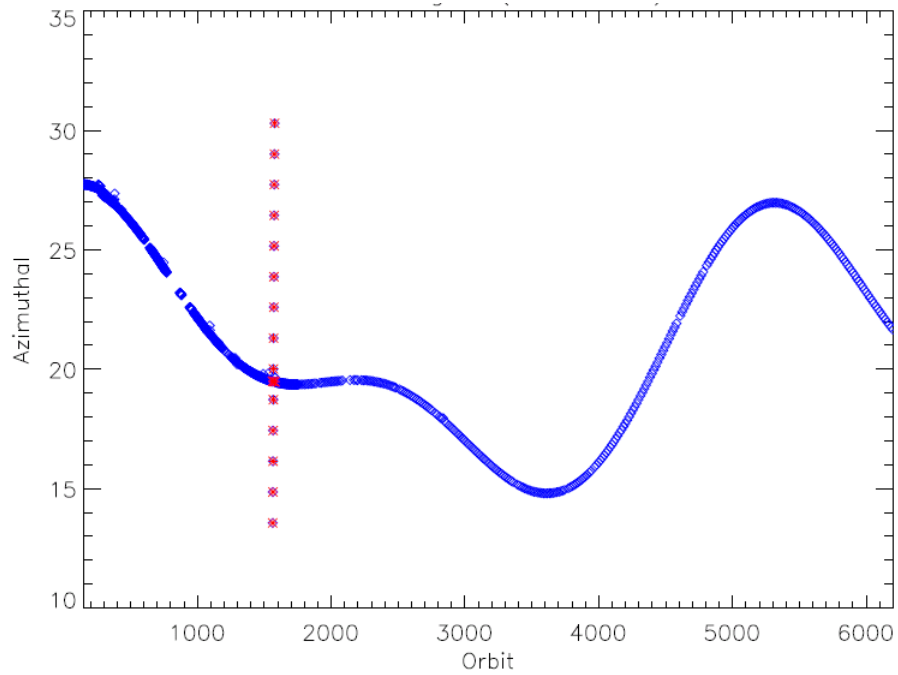


Figure 2: SDSM azimuth angle at 0 degrees SDSM elevation versus orbit. Data Set 1 is highlighted in green in the upper plot and Data Set 2 is highlighted in green in the lower plot. Yaw maneuver orbits are highlighted in red.

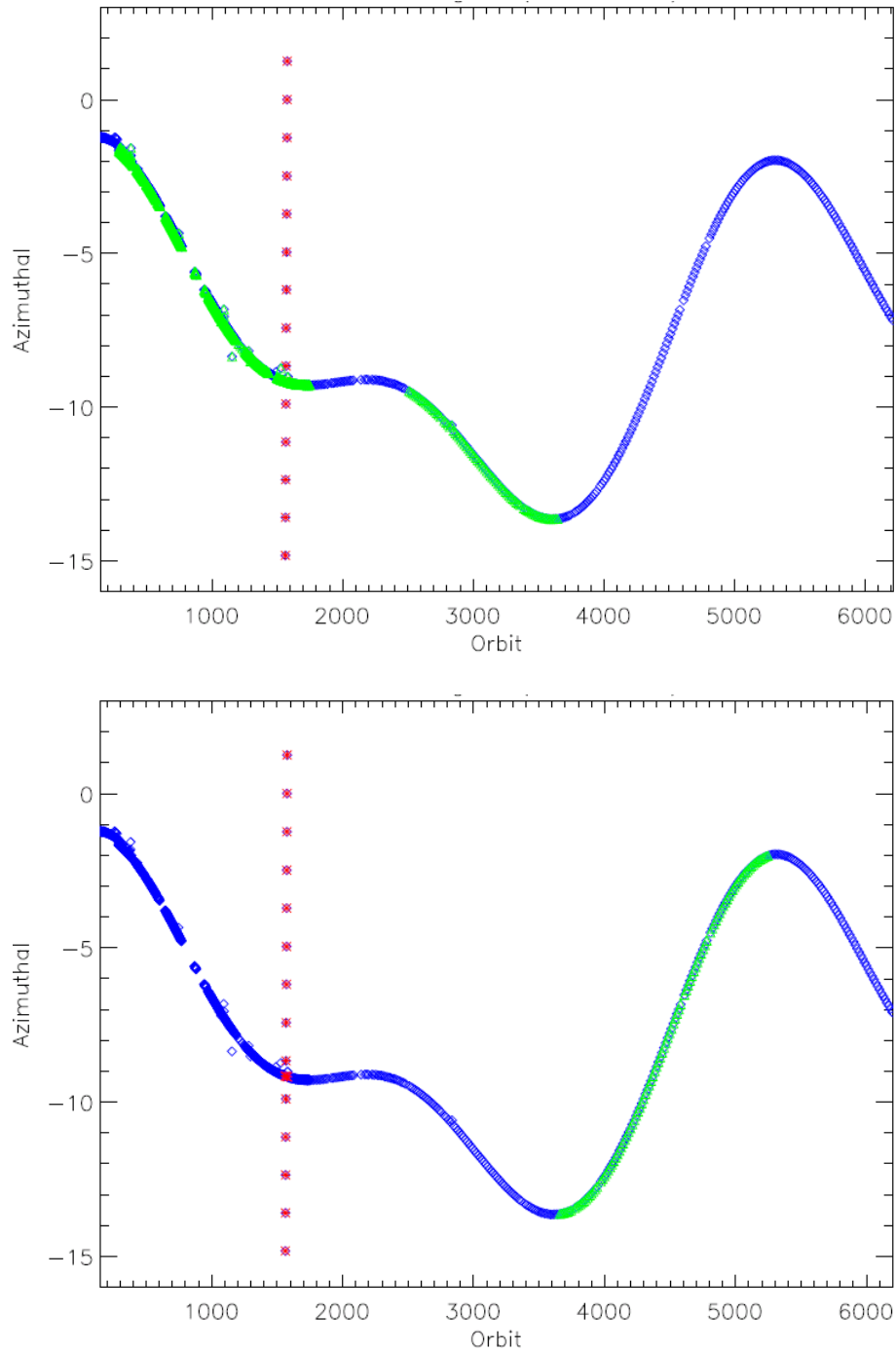


Figure 3: SDSM detector 1 current τ_{SDSM} (upper plot) and ratio of delivered [3] to current derived τ_{SDSM} (lower plot).

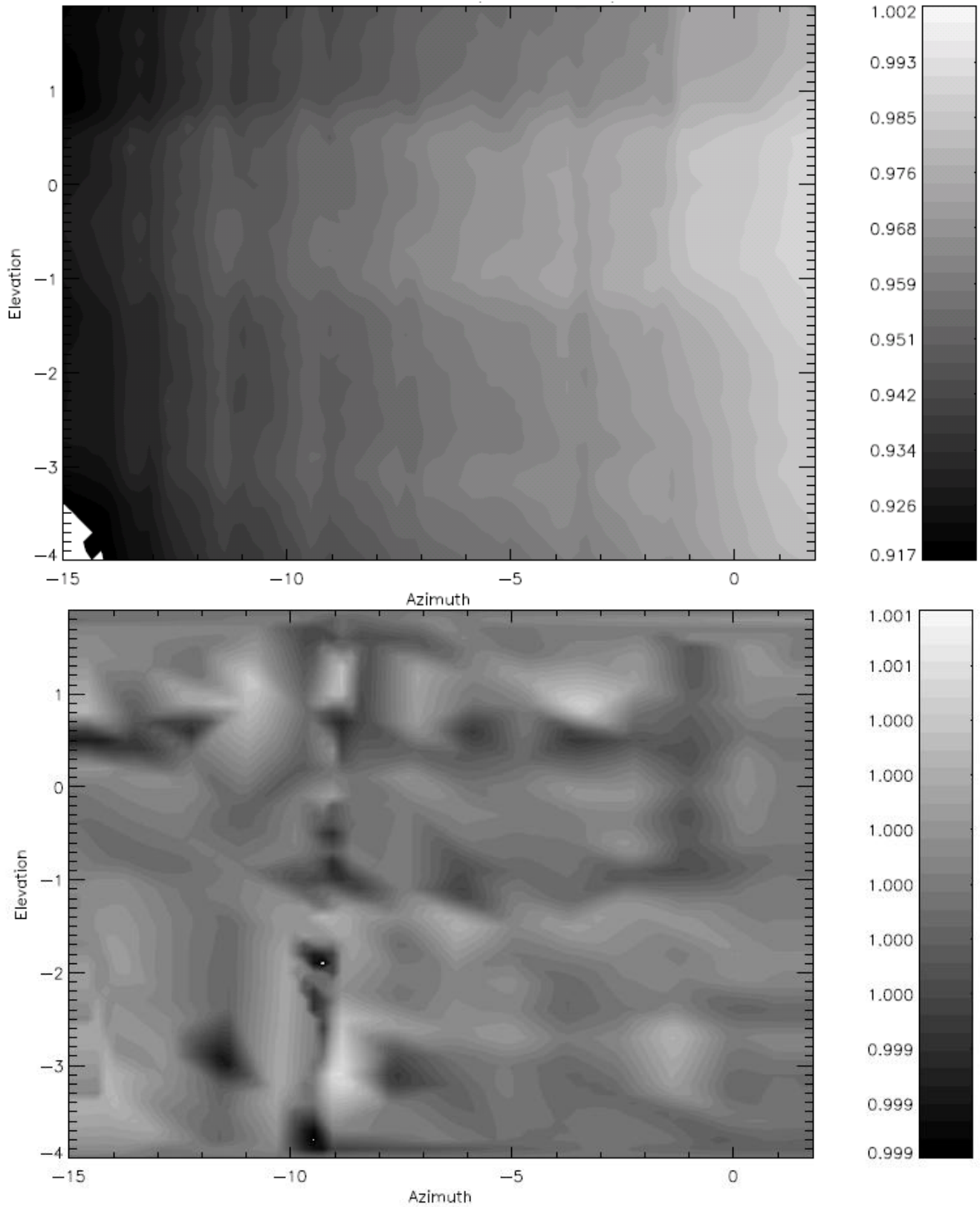


Figure 4: SDSM detector 2 current τ_{SDSM} (upper plot) and ratio of delivered [3] to current derived τ_{SDSM} (lower plot).

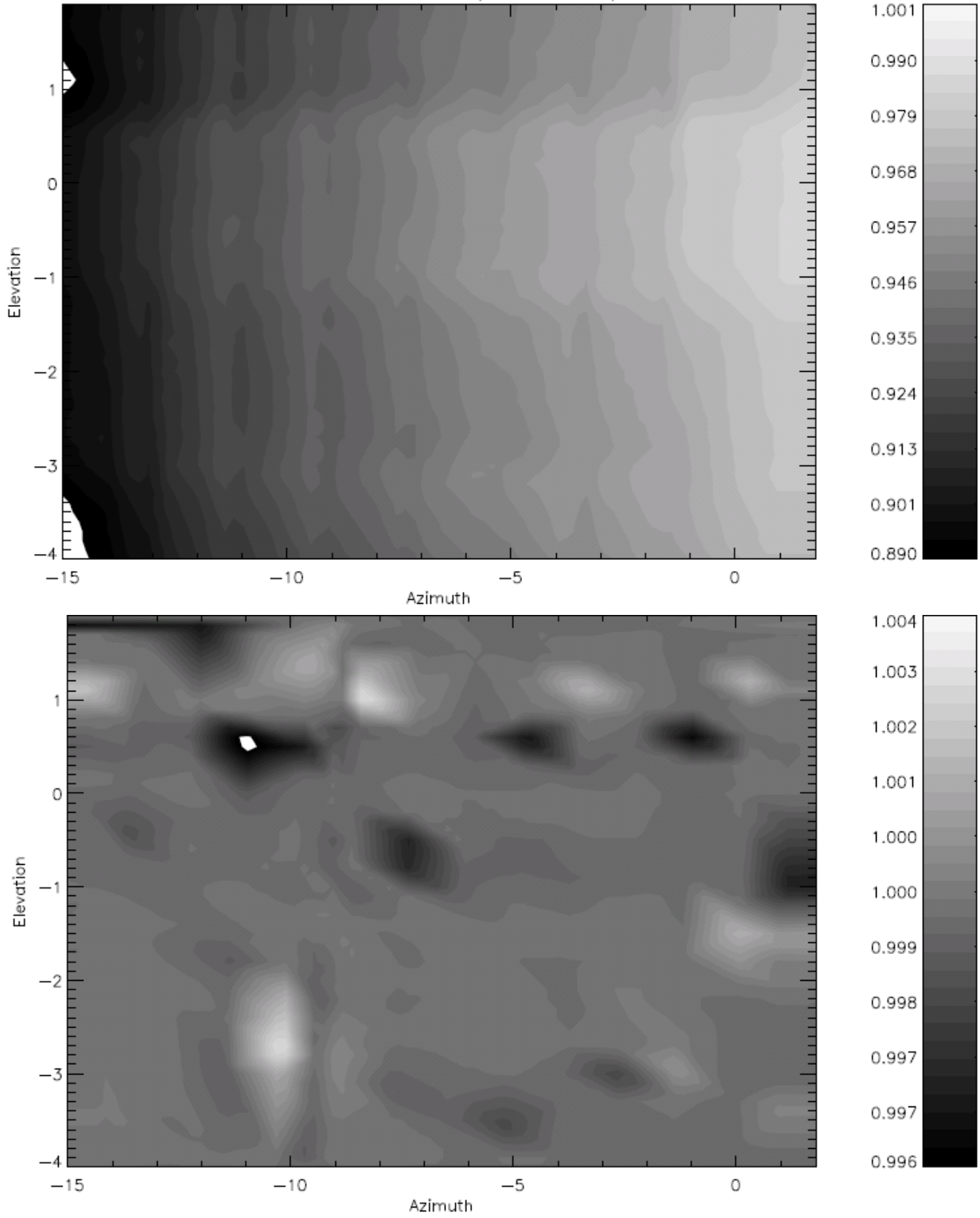


Figure 5: SDSM detector 3 current τ_{SDSM} (upper plot) and ratio of delivered [3] to current derived τ_{SDSM} (lower plot).

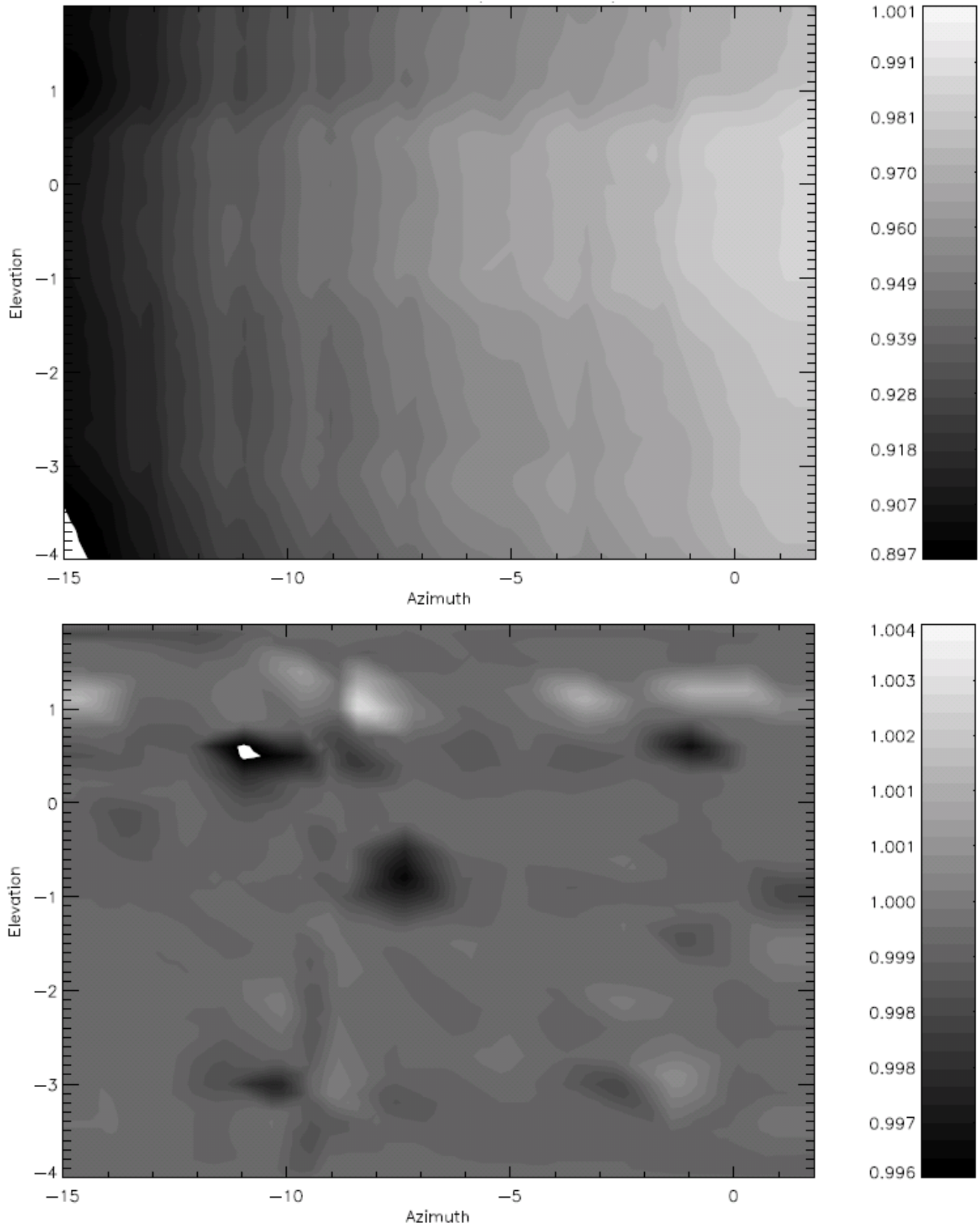


Figure 6: SDSM detector 4 current τ_{SDSM} (upper plot) and ratio of delivered [3] to current derived τ_{SDSM} (lower plot).

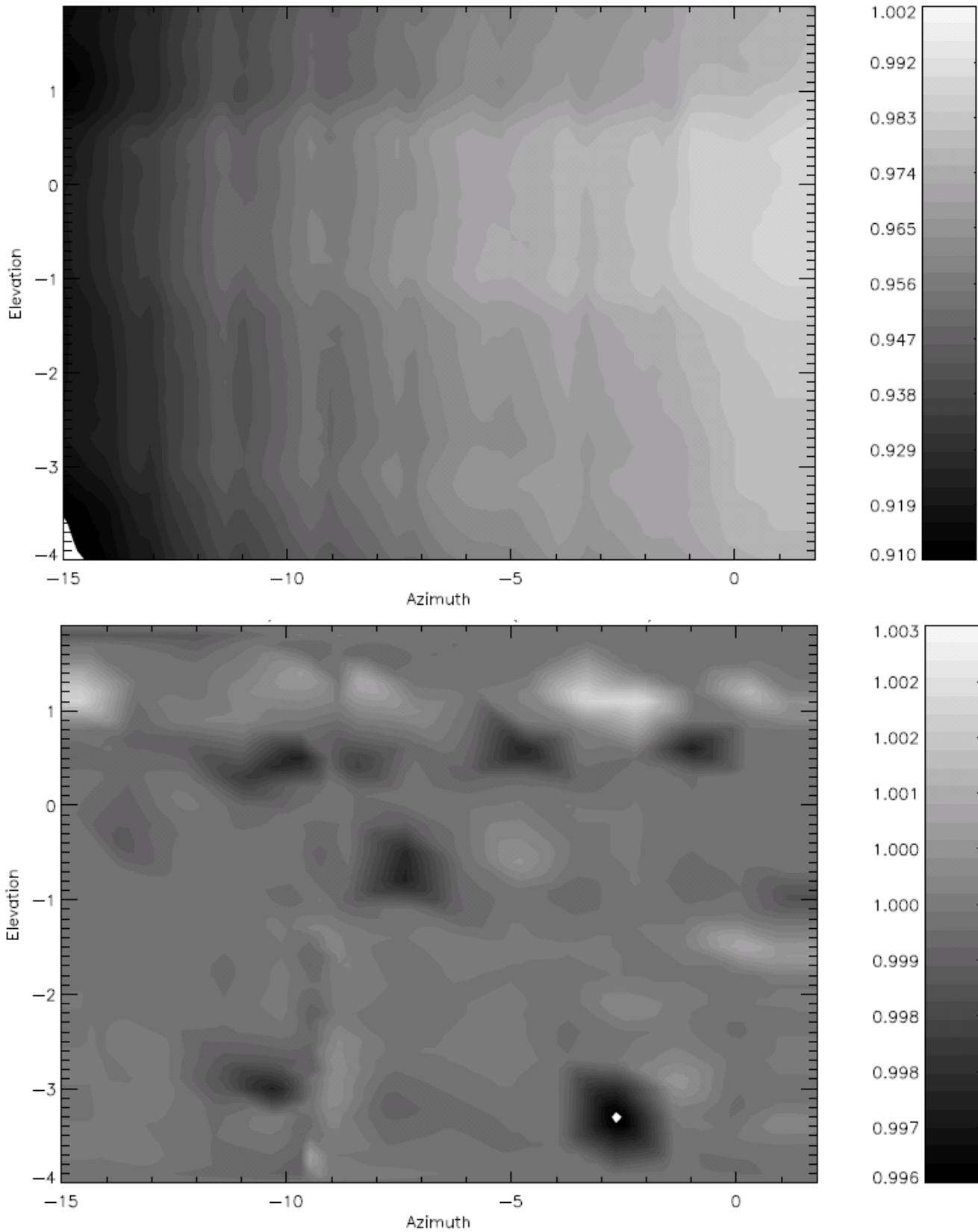


Figure 7: SDSM detector 5 current τ_{SDSM} (upper plot) and ratio of delivered [3] to current derived τ_{SDSM} (lower plot).

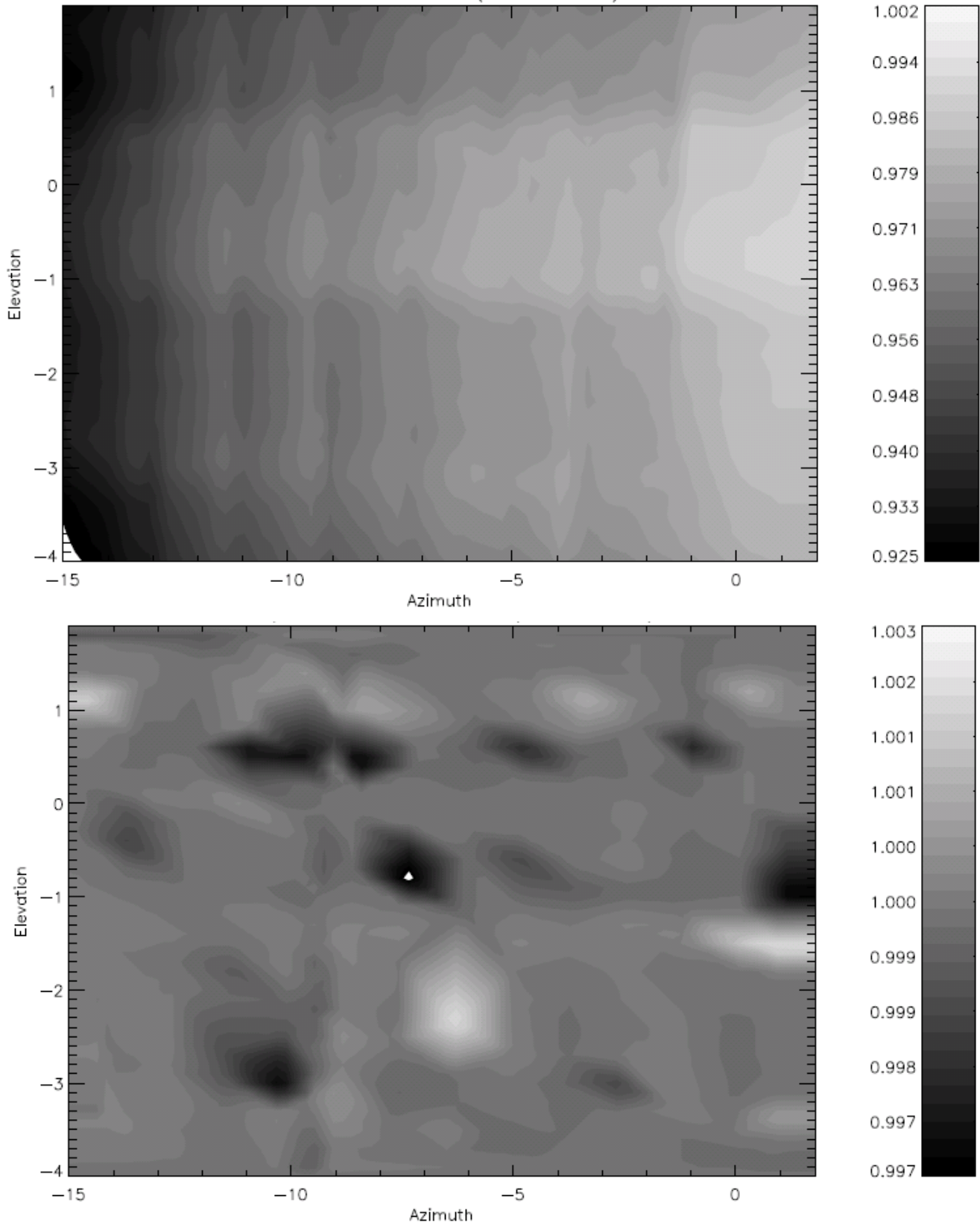


Figure 8: SDSM detector 6 current τ_{SDSM} (upper plot) and ratio of delivered [3] to current derived τ_{SDSM} (lower plot).

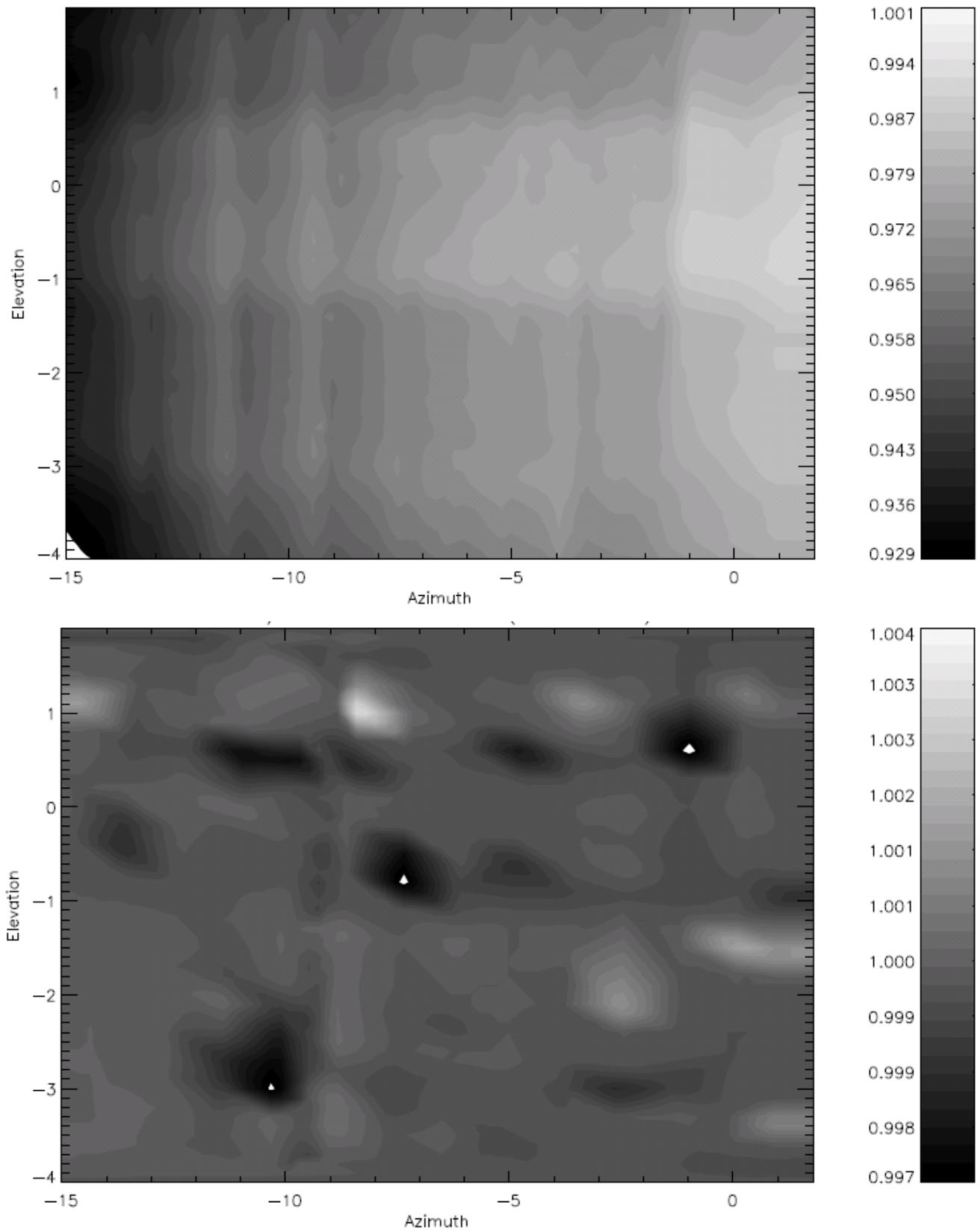


Figure 9: SDSM detector 7 current τ_{SDSM} (upper plot) and ratio of delivered [3] to current derived τ_{SDSM} (lower plot).

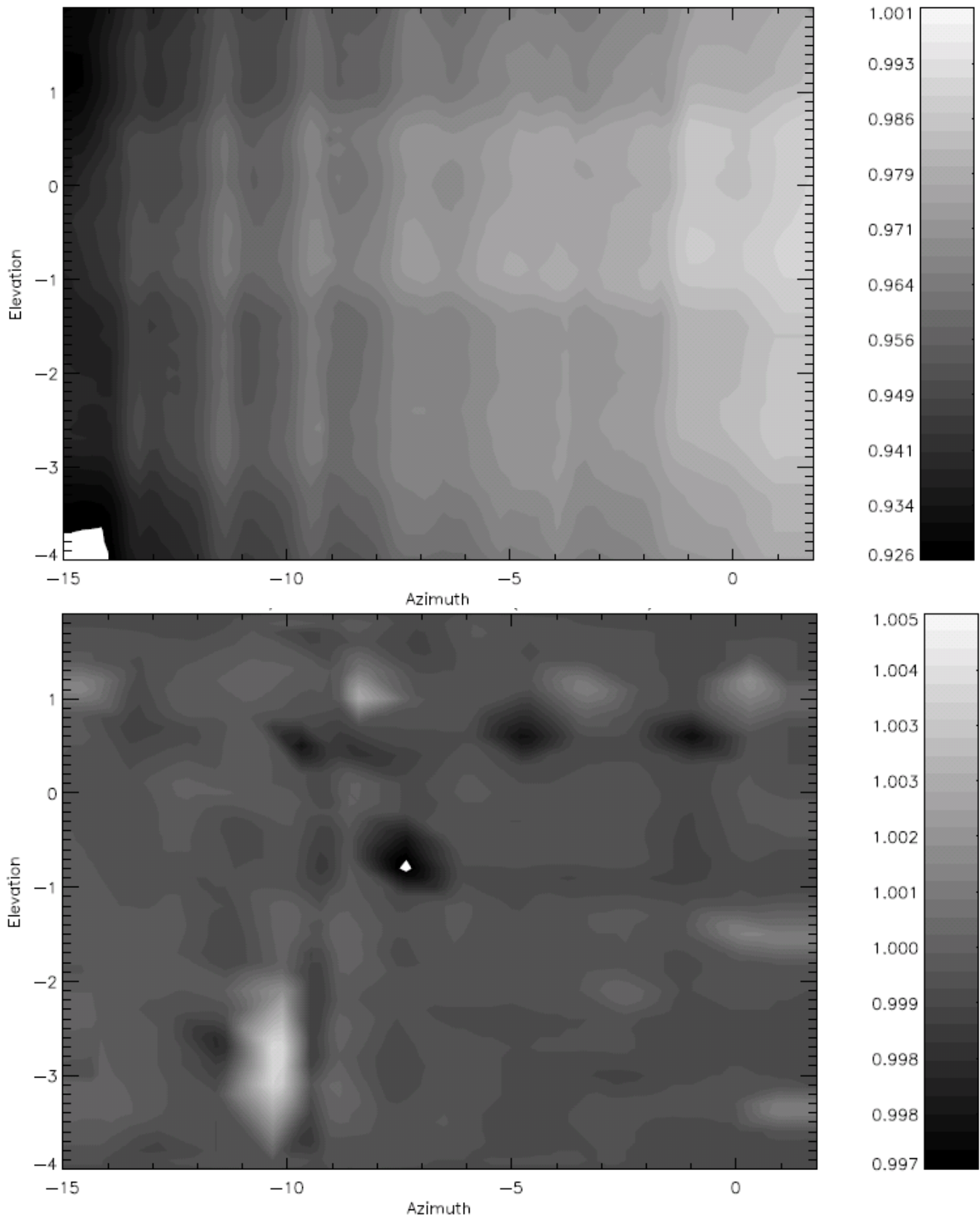


Figure 10: SDSM detector 8 current τ_{SDSM} (upper plot) and ratio of delivered [3] to current derived τ_{SDSM} (lower plot).

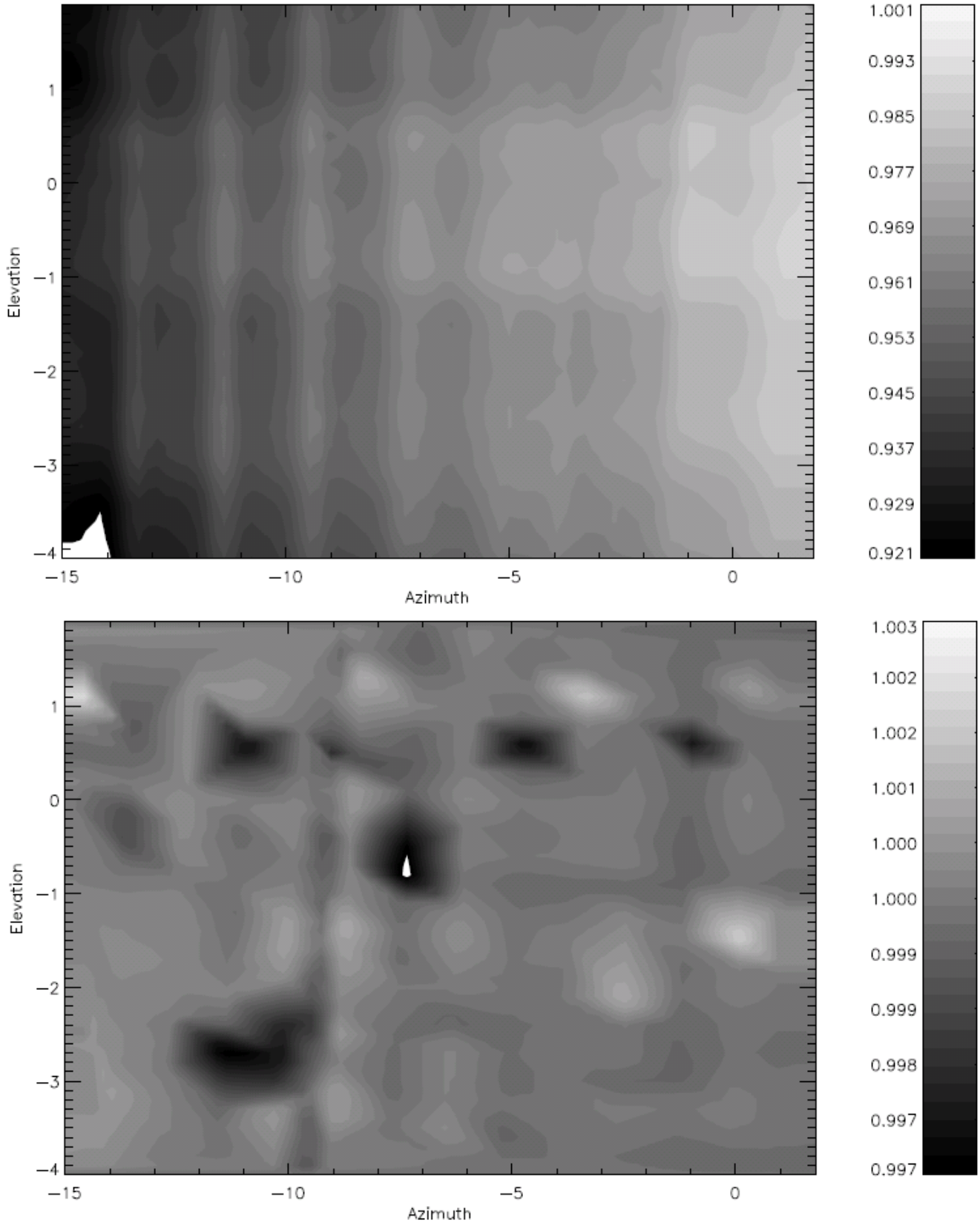


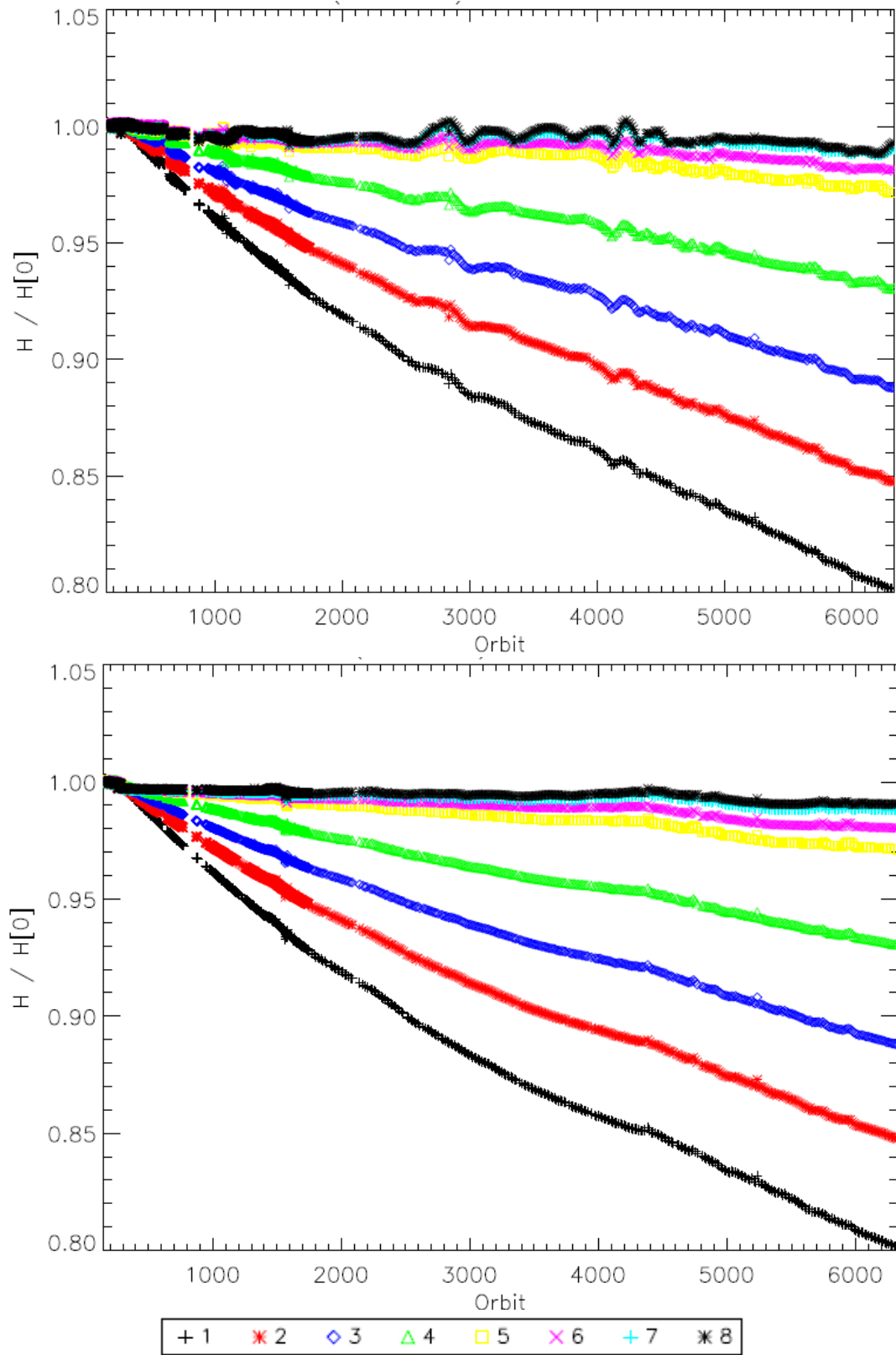
Figure 11: (H/H_0) over the entire mission for the delivered (upper plot) and derived (lower plot) τ_{SDSM} .

Figure 12: Ratio of delivered to derived H over the entire mission.

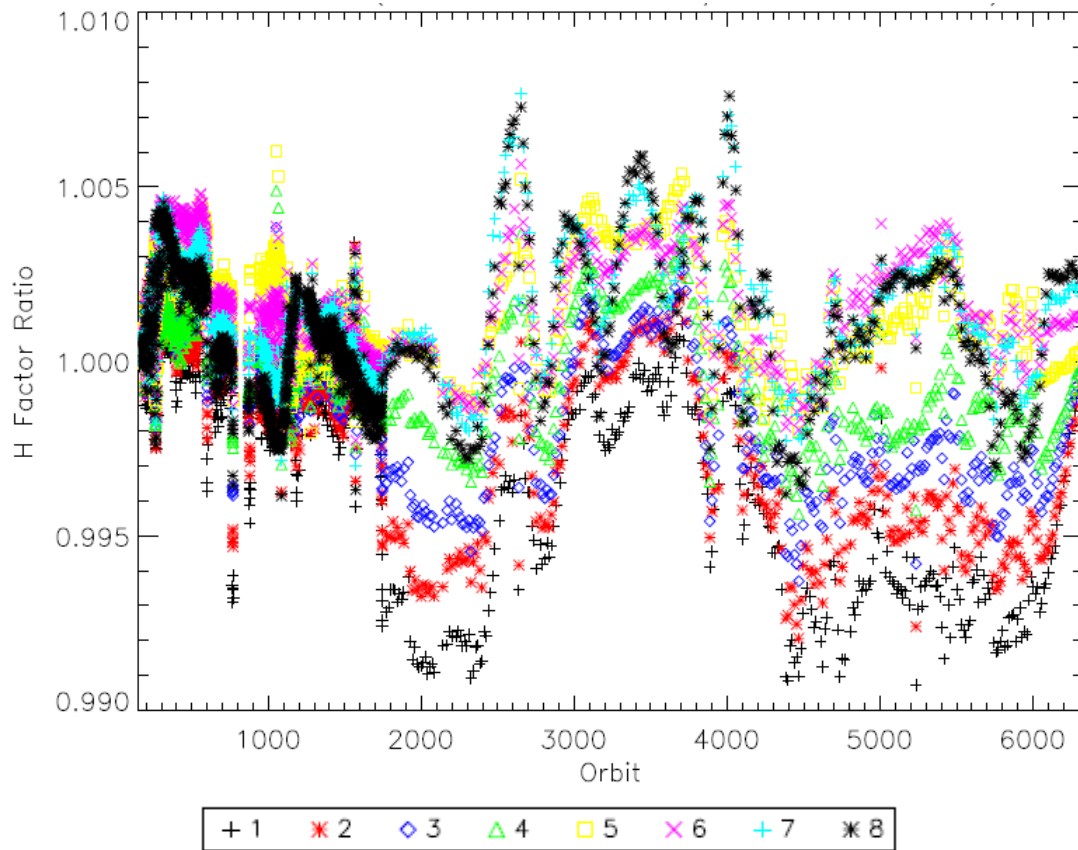


Figure 13: Scan-to-scan (H/H_0) for at-launch (black), delivered (red), and derived (blue) τ_{SDSM} for SDSM detectors 1 (upper plot) and 2 (lower plot).

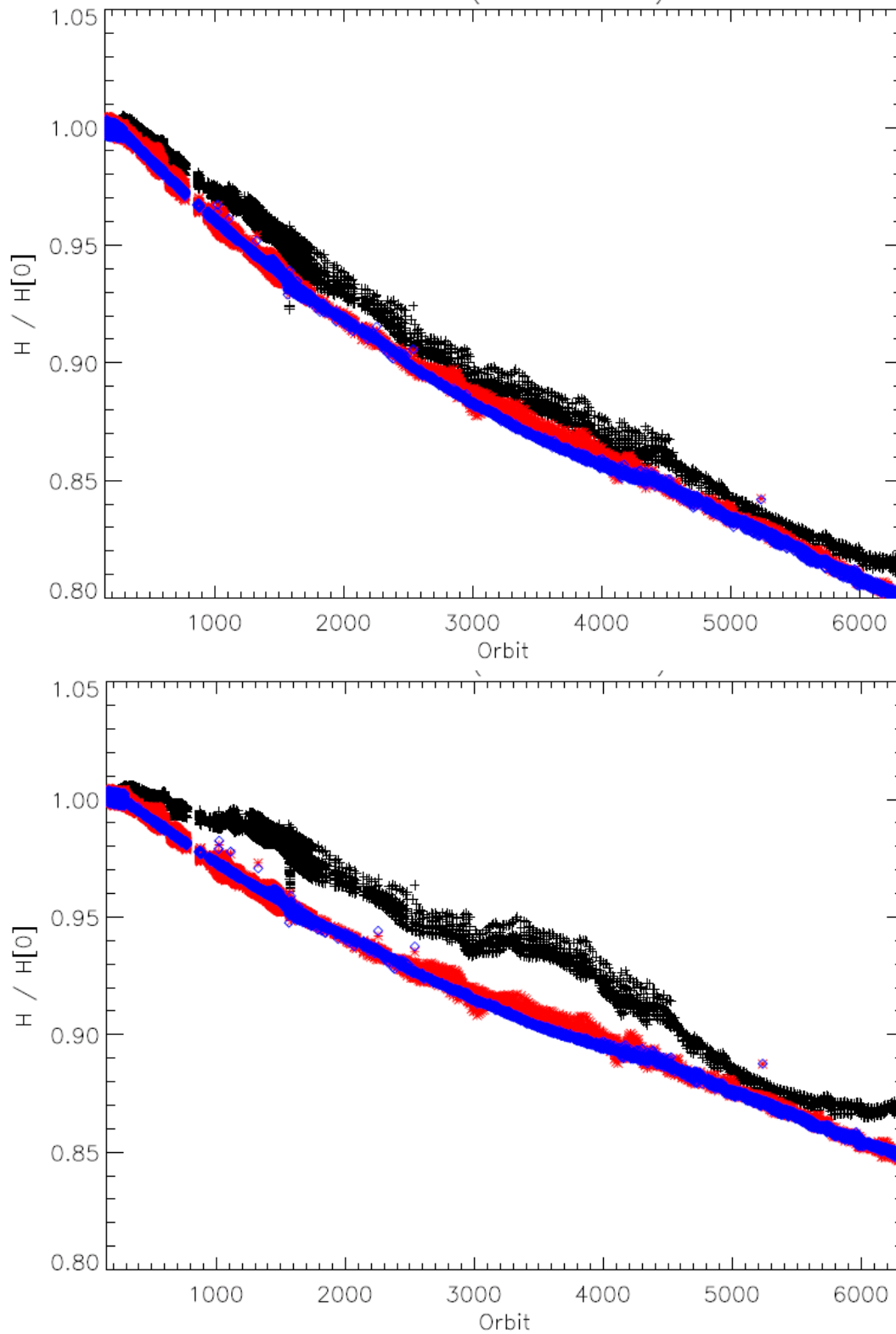


Figure 14: Scan-to-scan (H/H_0) for at-launch (black), delivered (red), and derived (blue) τ_{SDSM} for SDSM detectors 3 (upper plot) and 4 (lower plot).

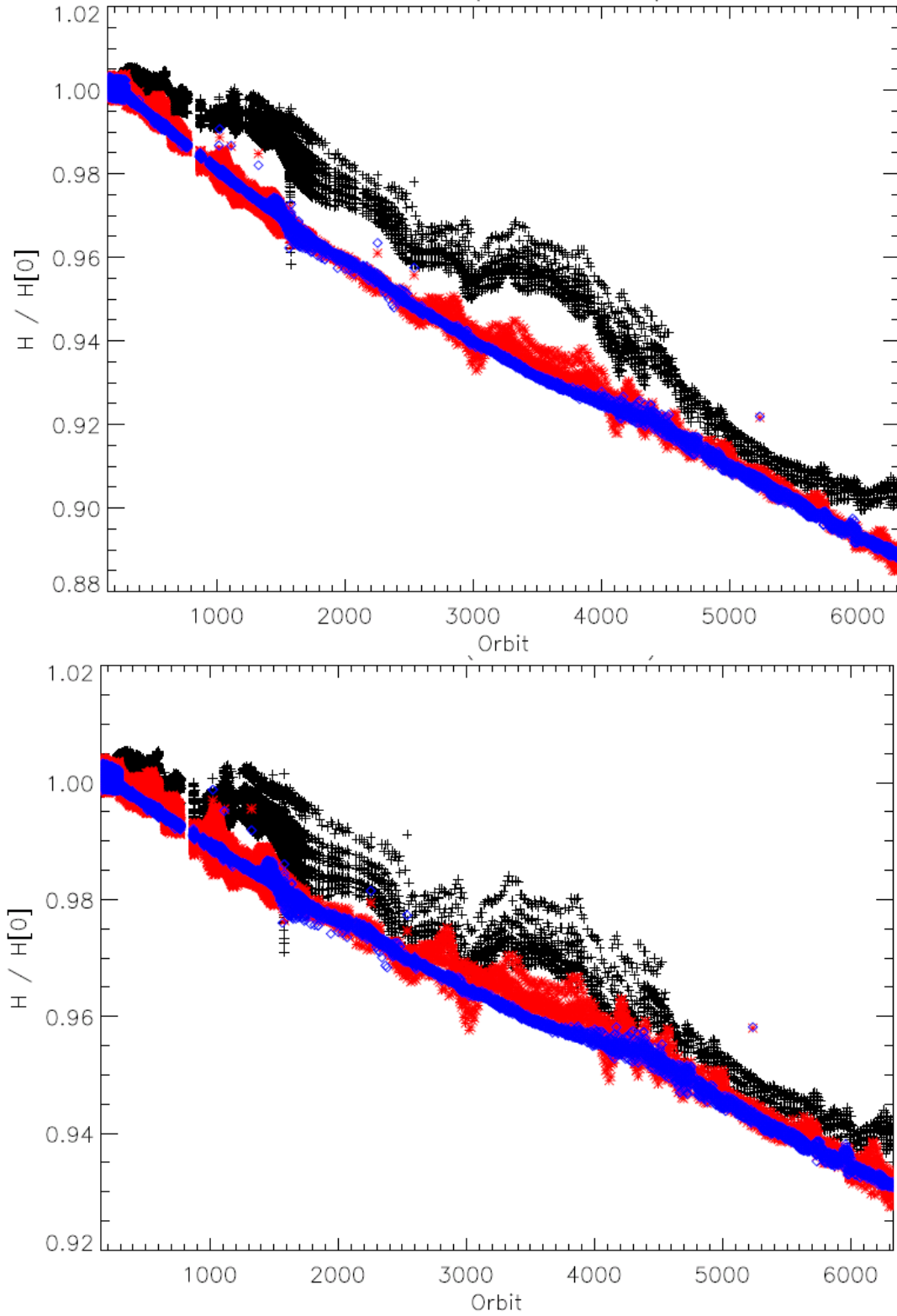


Figure 15: Scan-to-scan (H/H_0) for at-launch (black), delivered (red), and derived (blue) τ_{SDSM} for SDSM detectors 5 (upper plot) and 6 (lower plot).

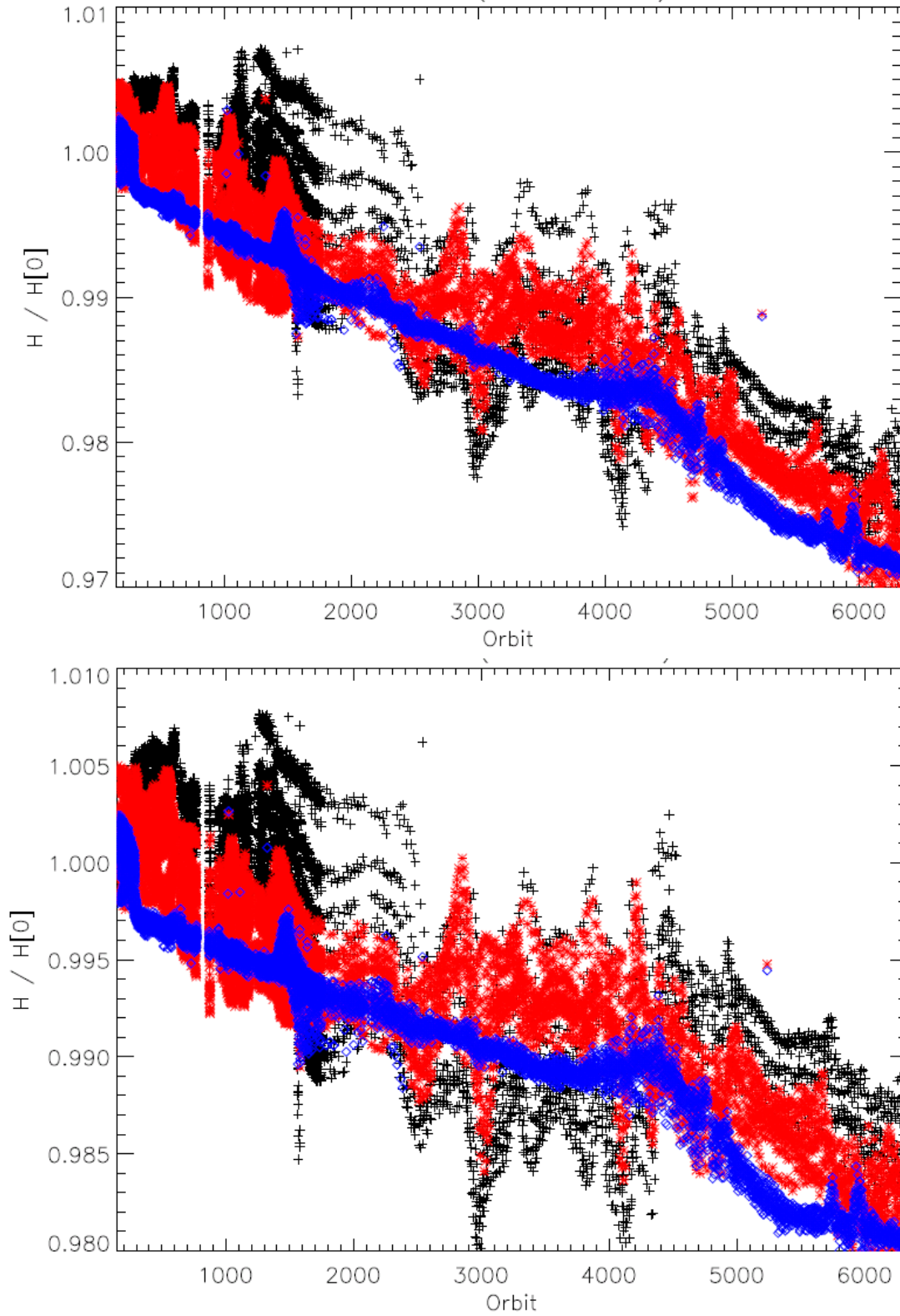


Figure 16: Scan-to-scan (H/H_0) for at-launch (black), delivered (red), and derived (blue) τ_{SDSM} for SDSM detectors 7 (upper plot) and 8 (lower plot).

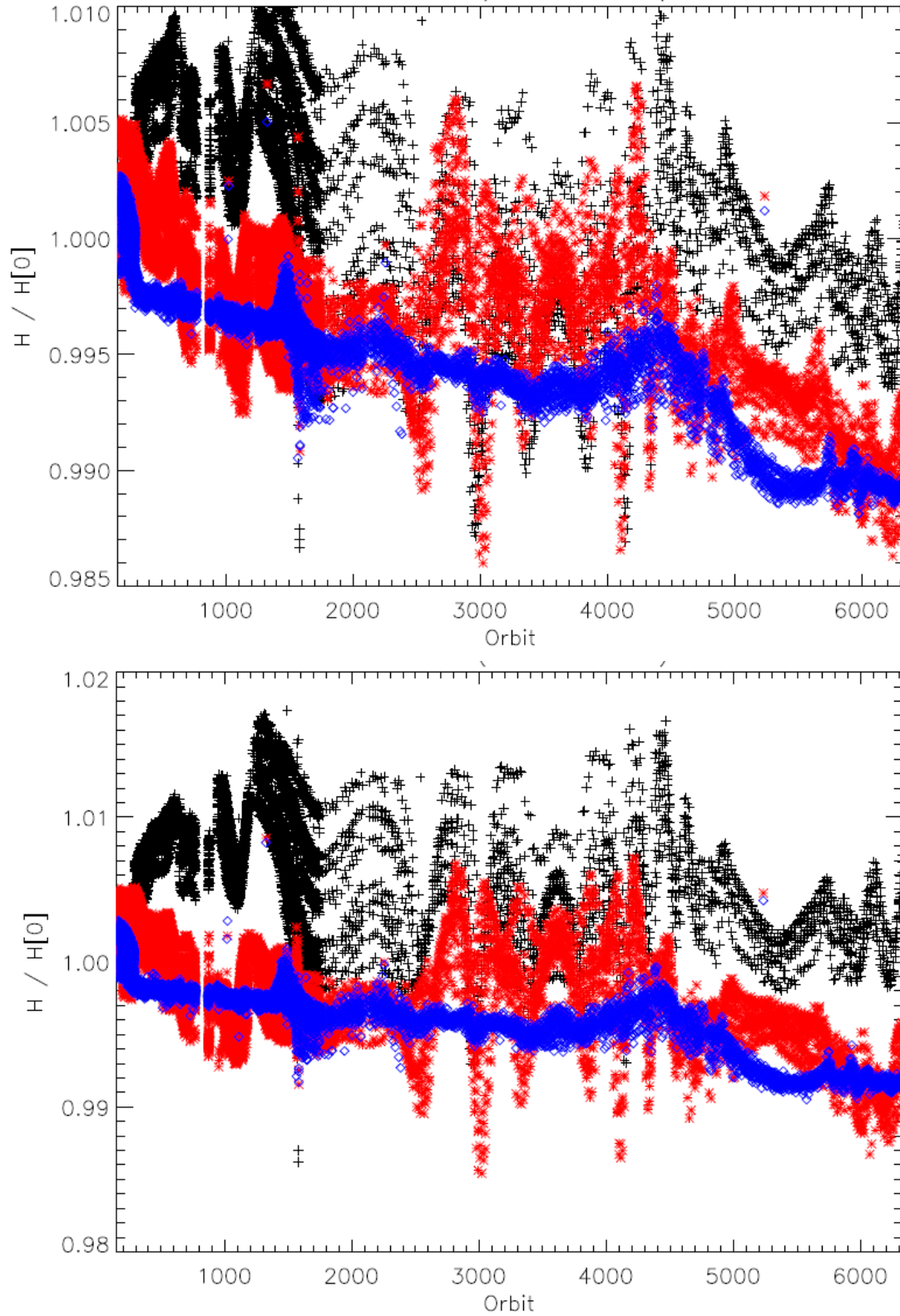


Figure 17: (H/H_0) over the entire mission for the derived τ_{SDSM} using data sets 1 and 2 (upper and lower plots respectively).

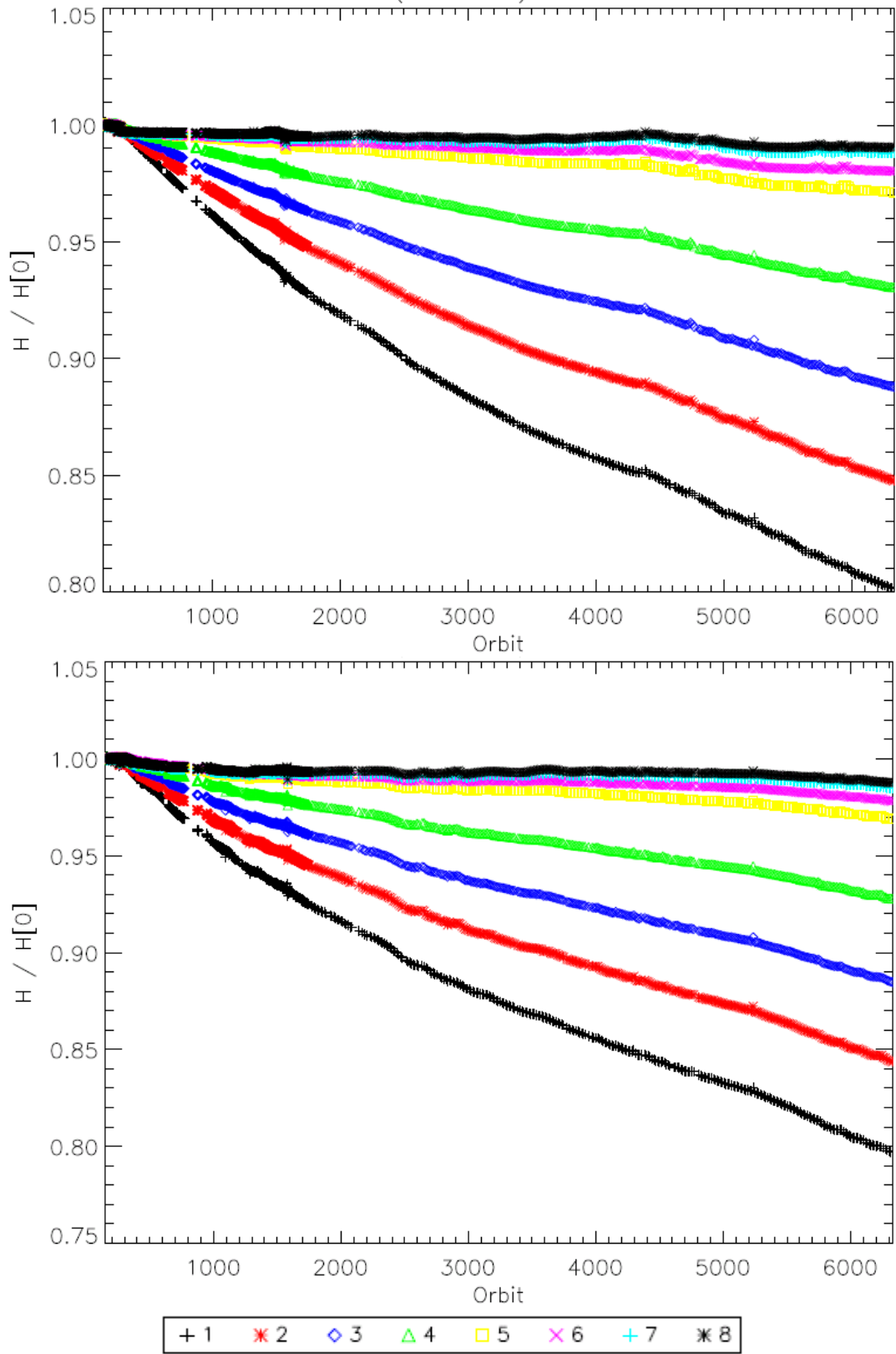


Figure 18: Ratio of the two derived H over the entire mission.

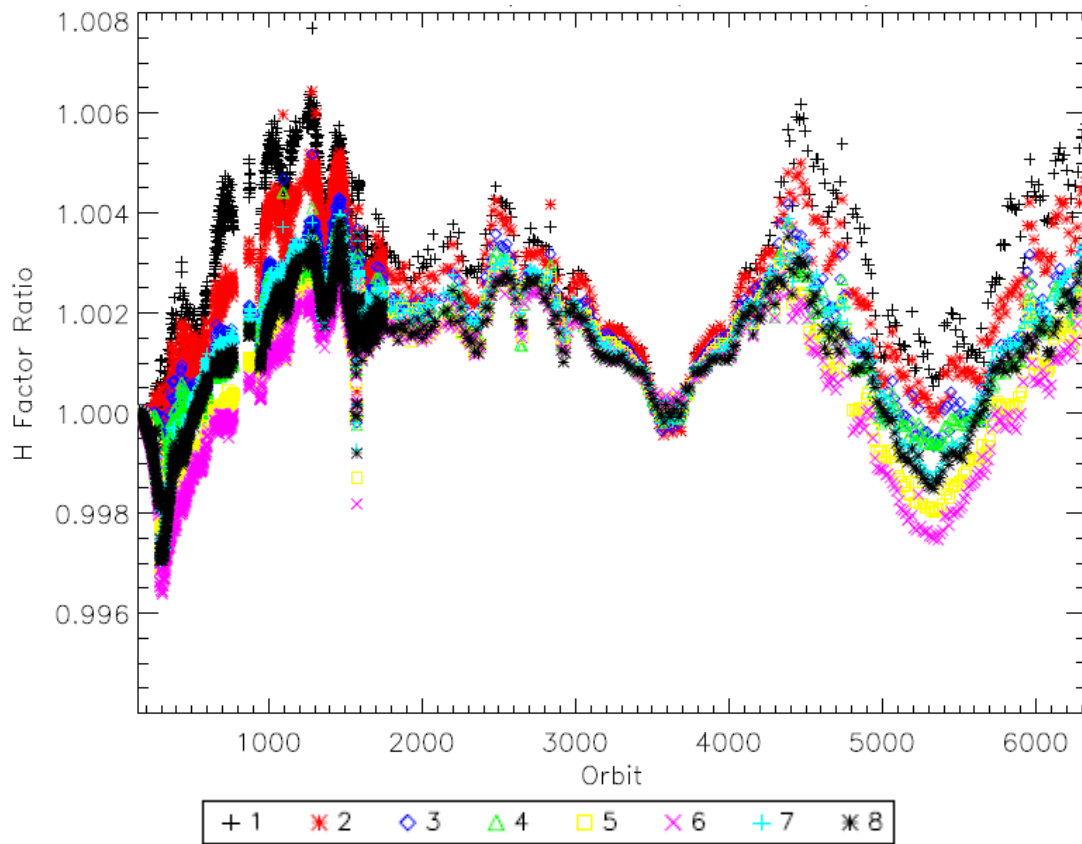


Figure 19: (H/H_0) for SDSM detectors 1 (upper plot) and 2 (lower plot) using the screen transmissions derived from data sets 1 and 2 (red and blue respectively). The (H/H_0) using the delivered screen transmission is shown in black.

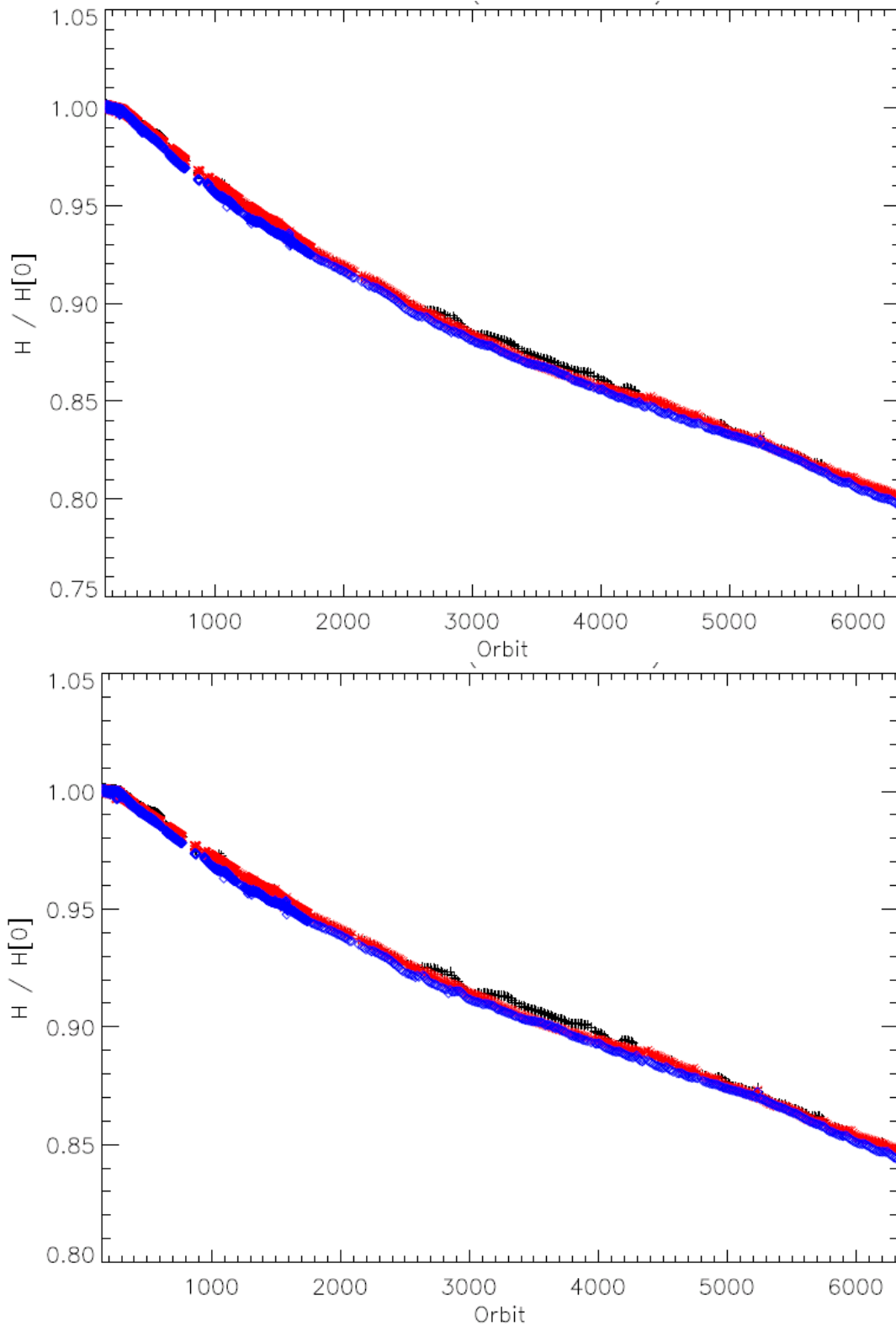


Figure 20: (H/H_0) for SDSM detectors 3 (upper plot) and 4 (lower plot) using the screen transmissions derived from data sets 1 and 2 (red and blue respectively). The (H/H_0) using the delivered screen transmission is shown in black.

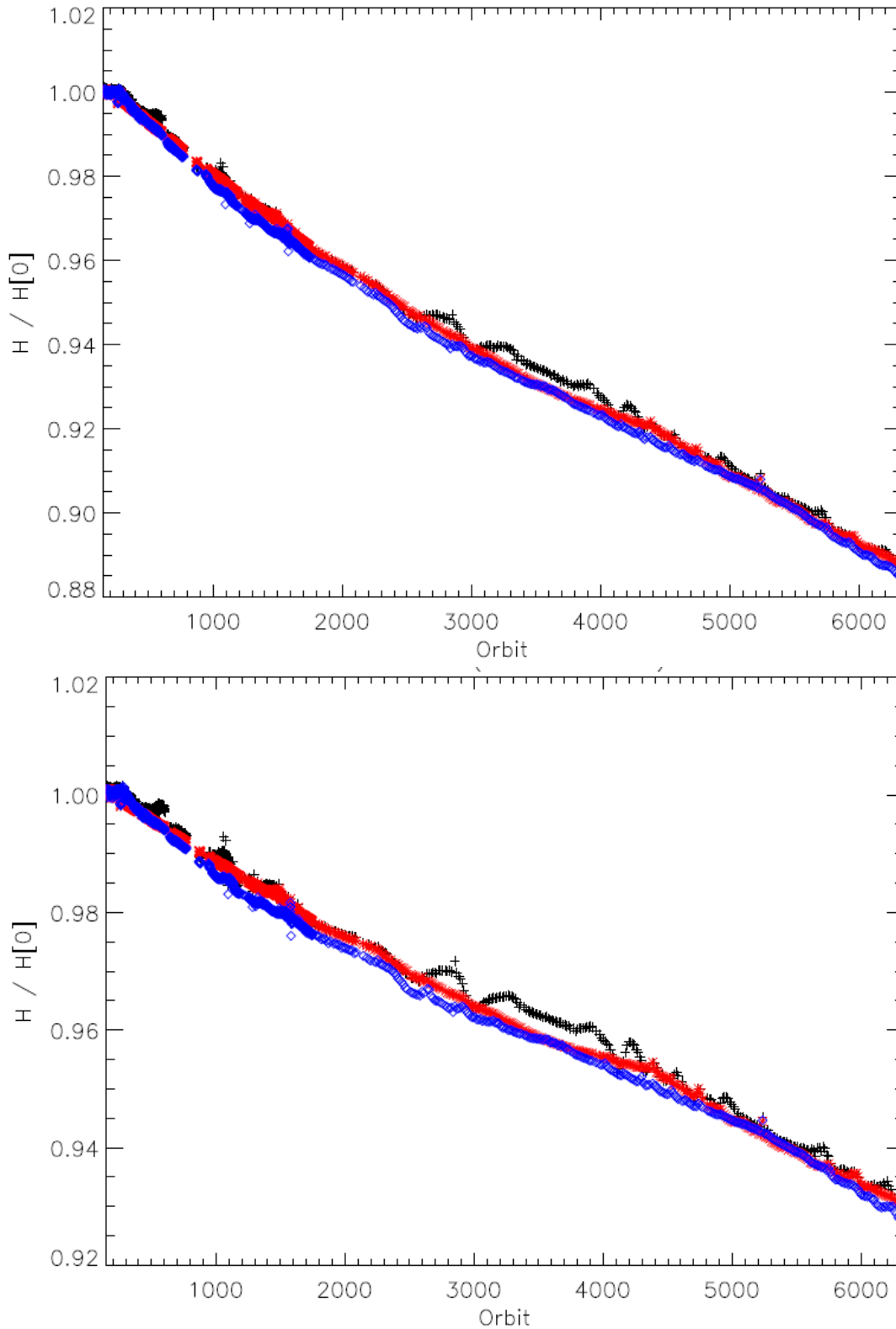


Figure 21: (H/H_0) for SDSM detectors 5 (upper plot) and 6 (lower plot) using the screen transmissions derived from data sets 1 and 2 (red and blue respectively). The (H/H_0) using the delivered screen transmission is shown in black.

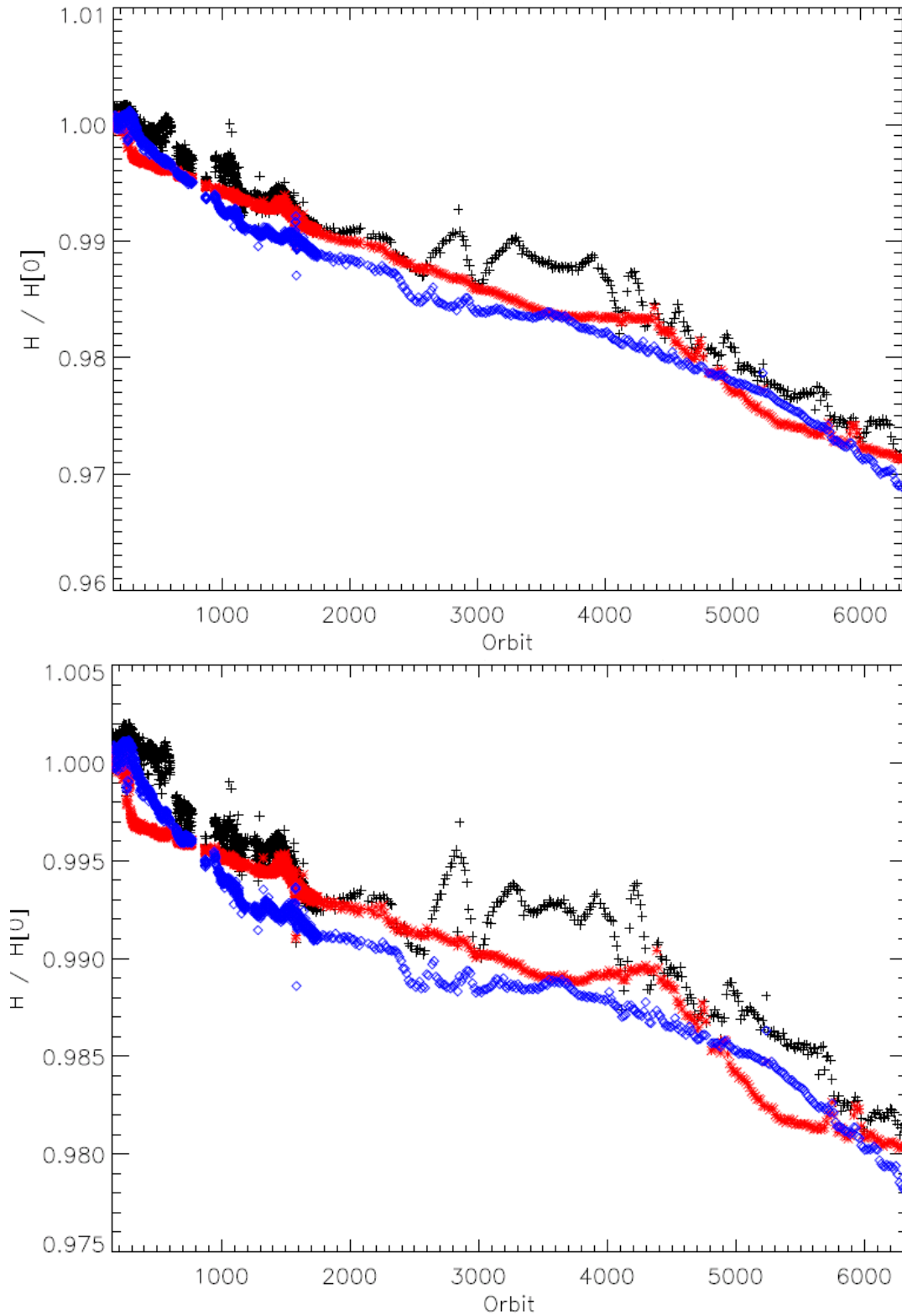


Figure 22: (H/H_0) for SDSM detectors 7 (upper plot) and 8 (lower plot) using the screen transmissions derived from data sets 1 and 2 (red and blue respectively). The (H/H_0) using the delivered screen transmission is shown in black.

